Modeling of Liquid Impingement Erosion on Compressor Blades

Progress report

Reporter: Mohsen N. Marzbali

Supervisor: Ali Dolatabadi

December 2011

Abstract

The dynamic response of a metallic disk to the impact of a liquid droplet is studied. In order to address the parameters that influence such a phenomenon, two solid materials are chosen for the disk, namely, martensitic stainless steel and Ti-6Al-4V. The impact velocity is varied from 10 to 40 m/s. The substrate is thin allowing the deformation of the disk during the impact; the thicknesses of 2.5, 5.0 and 10.0 mm are selected. Two droplet sizes of 0.5 and 1 mm in diameter are selected to investigate any dependence of the stress levels on the drop size. The pressure in the fluid region and the stress distribution in the solid part are obtained simultaneously by solving the coupled equations of motion. A 2-D axisymmetric model is utilized as the computational domain for fluid and solid parts. The deformation and spreading of the droplet upon impacting the solid surface are captured by Volume of Fluid (VOF) method. The pressure and stress distribution are investigated radially along the solid-fluid interface and axially along the center axis over time. The disk deflection at its center is monitored and compared for several cases.

Contents

1 Introduction

The liquid drop impact on an elastic solid is an interdisciplinary phenomenon as it involves both fluid dynamics and solid mechanics. Predicting the solid response to the droplet impact is of high importance in engineering applications and it requires capturing the flow features in the liquid accurately. Once the fluid variables and solid characteristics are resolved, then the solid elastic deformation caused by the liquid impact can be determined. In this chapter the analytical and numerical works reported in literature are presented. Next, a general overview of the problem of interest is reported herein.

1.1 Literature review

In 1927, Honegger [1] shed light on the mechanisms of solid erosion due to droplet impacts with series of experiments. He argued that no erosion is observed prior to the formation of roughness on the surface. After the incubation stage, the erosion rate grows rapidly as the droplets penetrate to the unevenness on the surface due to high pressure of the impact. In case of droplet impact on the rotating blades of a compressor with a very high relative velocity high transient stresses are generated in the material. Since the impingements are consecutive, fatigue causes the material to spall off from the blade surface. After this period, a layer of liquid forms on the surface and fills the gaps in the solid. As a result, the impinged droplets do not impact the solid directly and the destruction of the surface is reduced.

Upon impact of liquid droplets onto a solid, elastic deformation occurs in the layers of the substrate close to its surface. Cyclic pressure pulses created by impingements of liquid droplets onto the surface develop and propagate cracks causing cratering and the material loss via ductile rupture according to Bargmann [2]. The craters change the surface topography; hence, the hydrodynamic loading on the surface varies during frequent impingements of the droplets as the impact angle changes. Consequently, the material behavior alters in response to the repetitive impact loading and the work hardening on the surface. Bargmann [2] stated that liquid impingement erosion is dependent on space and time; hence, it can be expressed as a stochastic process. In this regard, the diameter distribution of the droplets, the, impact velocity, the frequency of impingements and the location of drop impacts are needed to solve the fluid-solid problem simultaneously. Once the space and time variation of the pressure field in the liquid and the stress field in solid are obtained, the damage can be predicted by carrying out the fatigue analysis on the solid as explained in reference [3].

The first liquid-solid model was proposed by Honegger [4] in 1927 where a liquid jet impacts a solid wall creating a constant pressure known as the water hammer pressure. After him, Cook [5] and Engel [6] reported the 1-D steady state solution for the water hammer pressure. Blowers [7] proposed another pressure model to obtain the stress field in the rigid solids, however, uncoupled to the pressure field in the liquid. In addition to analytical methods, numerical simulations have been used to model droplet impact on solid substrates at high velocities. For instance, Adler and Mihora [8] utilized Finite Element Method to study water droplet impact onto solid at a high velocity. Moreover, several detailed analyses were done to simulate high speed impact of droplets on solids such as Haller *et al.* [9] and Huang *et al.* [10].

In general, solving the liquid-solid problem can be divided into two main categories: one-way coupling and two-way coupling of liquid and solid equations. In the first approach, the pressure field in the liquid is solved via analytical or numerical tools and then used as a boundary condition on the solid to obtain the stress field, e.g. the work reported by Shih [11]. The main

drawback of this method is that it underestimates the maximum stress magnitude and is not able to capture its location. It should be mentioned that the peak transient stress is much higher than its steady state value and is responsible for the solid erosion according to Chen *et al.* [12]. This approach was improved later by researchers like Kim *et al.* [13] and Lee *et al.* [14] by replacing the pressure distribution on the solid surface with point loads. Although more accurate, their approach does not reflect the dynamic pressure variation of the liquid on the stress in the solid since the fluid and solid equations were segregated in their model.

On the other hand, in the two-way coupling approach, the space and time variation of the stress in the solid is directly coupled with spatial pressure history in the liquid droplet. This method allows predicting the transient stress produced by the pressure imposed on the liquid-solid interface. In 2008, a fully coupled Fluid-Solid Interaction model in one dimension was reported by Li *et al.* [15] via linear and nonlinear methods for rigid and elastic solids. The 1-D numerical model developed by Li *et al*. [15] was further extended to 2-D axisymmetric model by Zhou *et al*. [16] since the shock wave propagation cannot be described precisely in one dimension. They utilized the elastodynamic equation to solve the solid displacement and cell marking method to separate the gas, liquid, and solid phases in the computational domain. They assumed that the droplet impacts are independent of previous impacts and the drop sizes do not affect the influence zone. They used Soderberg's fatigue model [17] to carry out the erosion analysis for repetitive impacts on steam turbine blades and find the blade life time. They concluded that the inner arc of the turbine blade experiences more erosion than its back arc since the impact speed is higher in that region.

1.2 Overview

The liquid droplet impact on solids was addressed in several experimental studies in the past. Furthermore, theoretical and numerical tools were used extensively to model the fluid dynamics of the impact. Other methods were proposed to calculate the stress in the solid material separate from the liquid by applying the pressure force on the solid surface (one-way coupling). It has been shown in the previous works that using one-way coupling approach results in underestimation of transient stress in the solid. Hence, two-way coupling of the liquid-solid equations is essential in finding the accurate stress distribution in solid over time. 1-D and 2-D axisymmetric analyses with full coupling of liquid-solid impact have been completed for the duration of 100 ns after the impact. The 2-D axisymmetric model resolves the contact edges of the droplet and captures the shock wave front better than 1-D model. In general, the 2-D model provides more information about the maximum stresses and the locations where they appear in the solid compared to the 1-D model. It should be remembered that a 3-D model to simulate droplet-solid interaction is still missing in the open literature. It has been discussed that the maximum transient stress is much larger than its steady state value, and hence more important for the liquid-solid problem. To address this issue the pressure history in the liquid drop needs to be obtained accurately both in loading and unloading stages. Formation of lateral jets and droplets breakup were not considered in the model of Li *et al.* [15] since they only focused on the acoustic stage of the impact where the drop deformation is negligible. However, it is shown that the loading step where maximum compressive stress appears in the material is followed by an unloading stage when tensile stress is observed in the solid. Although the tensile stress has lower magnitude that the compressive stress it can cause severe damage to the blade via fatigue if the impact frequency is high. In this study both loading and unloading stages are modeled by

capturing the droplet deformation and breakup during the impact. The methodology is implemented first followed by results section. The last part concludes the results obtained in this work.

2 Methodology

In this chapter the governing equations are presented in detail followed by the computational domain used for modeling. Finally, the initial and boundary conditions needed to solve the equations are outlined.

2.1 Governing equations

Navier-Stokes equations are solved for incompressible and Newtonian fluid as follow,

$$\nabla \cdot V_f = 0 \text{ in } \Omega_f \qquad \textbf{Eq. 2-1}$$

$$\rho_f \frac{\partial V_f}{\partial t} + \rho_f (\nabla V_f) V_f = \nabla \cdot \sigma_f + \rho_f g \text{ in } \Omega_f \qquad \textbf{Eq. 2-2}$$

V_f is the fluid velocity vector, ρ_f is the fluid density and σ_f is the stress tensor defined as,

$$\sigma_f = -p_f I + \rho_f \nu_f \left(\nabla V_f + \nabla V_f^{\,T}\right) \qquad \textbf{Eq. 2-3}$$

where p_f is the fluid pressure and ν_f is the fluid kinematic viscosity.

Volume of fluid (VOF) method is employed to capture the droplet interface with gas. In VOF, a scalar field is defined for volume fraction of liquid phase and its value depends on the fraction of the cell volume occupied by this phase indicated by α_l,

$$\begin{cases} \alpha_l = 0 & \textit{Gas phase} \\ 0 < \alpha_l < 1 & \textit{Gas} - \textit{liquid Interface} \\ \alpha_l = 1 & \textit{Liquid phase} \end{cases} \qquad \textbf{Eq. 2-4}$$

The values between zero and one denote the interface between gas and liquid phases. Since the volume fraction represents the volume occupied by the liquid, it should be advected by the flow field at each time step. The following equation governs the liquid advection of α_l,

$$\frac{\partial \alpha_l}{\partial t} + \nabla.(V_f \alpha_l) = 0 \qquad \textbf{Eq. 2-5}$$

Following the advection, the interface is reconstructed using the Piecewise Linear Interface Calculation (PLIC) proposed by Youngs [18]. In PLIC method, the interface is defined at each computational cell by a slope and an intercept. The slope of the interface is calculated based on the volume fractions of neighboring cells.

The fluid flow in all the simulations is assumed to be laminar; hence, no turbulence model is employed in the solver.

The structural equation for a elastic and deformabale solid is as follow,

$$\rho_s \frac{\partial V_s}{\partial t} + \rho_s (\nabla V_s) V_s = \nabla \cdot \sigma_s + \rho_s g \text{ in } \Omega_s \qquad \textbf{Eq. 2-6}$$

Where ρ_s is the solid density, V_s is the solid velocity which is equal to $V_s = \frac{\partial U_s}{\partial t}$ and U_s is the solid displacement. σ_s is Cauchy stress tensor described below,

$$\sigma_s = \frac{1}{J} F\left(\lambda_s (trS) I + 2\mu_s S\right) F^T \quad \textbf{Eq. 2-7}$$

Where J is determinant of F and F is the deformation gradient tensor defined as,

$$F = I + \nabla U_s \quad \textbf{Eq. 2-8}$$

S is obtained from St. Venant-Kirchhoff law,

$$S = \frac{1}{2}\left(F^T F - I\right) \quad \textbf{Eq. 2-9}$$

λ_s and μ_s are Lamé coefficients defined below,

$$\mu_s = \frac{E}{2(1+\nu_s)} \quad \textbf{Eq. 2-10}$$

$$\lambda_s = \frac{\nu_s E}{(1+\nu_s)(1-2\nu_s)} \quad \textbf{Eq. 2-11}$$

where ν_s and E are Poisson ratio and Young's modulus, respectively.

The coupling between fluid and solid is enabled with stress and velocity constraints at the interface, $\Gamma_0 = \Omega_s \cap \Omega_f$. The force balance and no slip condition on the interface Γ_0 imply,

$$\sigma_s n = \sigma_f n \quad \text{on } \Gamma_0 \quad \textbf{Eq. 2-12}$$

$$V_s = V_f \quad \text{on } \Gamma_0 \quad \textbf{Eq. 2-13}$$

where n is the unit normal vector to the interface, Γ_0. The detailed methodology can be found in reference [19].

2.2 Computational domain

The impact of a spherical liquid droplet onto a solid disk is modeled. The fluid and solid equations are solved over 2-D axisymmetric domains schematically shown below,

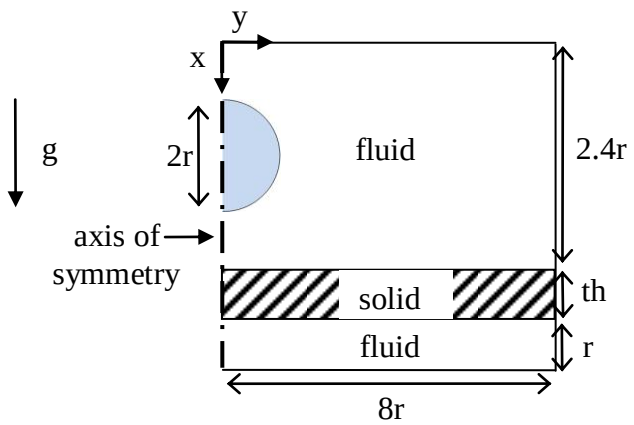

Figure 2-1: schematic presentation for 2-D axisymmetric model of droplet impact (not to scale).

The solid domain is placed between two fluid domains to allow the disk deformation. The x-axis is taken as the axis of symmetry and the droplet is patched around this axis at a distance 2r above the substrate. The disk thickness, th, varies for different cases. the heights of first and second fluid regions are 4 and 1 times the drop radius, respectively. The radius of both domains is set to 8 times the drop radius. The gravity force is exerted in positive x direction. The mesh is uniformly distributed in both domains with a grid size of 25 microns. The time step is adaptive and defined based on CFL condition,

$$CFL = \frac{\Delta t.V_f}{\Delta x}$$

The open source code OpenFoam is used as the computational solver. The fluid and solid parts are solved with interFoam and stressedFoam, respectively.

2.3 Initial and boundary conditions

At the beginning of each computation the droplet is patched in the fluid domain with the desired size and velocity. The computation for the rest of the cells starts with zero for all other variables. Outflow boundary condition is applied to all fluid edges that are not in contact with the solid. No-slip condition is imposed on the interfaces between fluid and solid. The solid is free to move except at its right edge (at y=8r) which is fixed to a wall.

3 Results and discussions

In this section the properties for the fluids and solids that are used for simulation are tabulated. A test matrix is then created to study the effect of various parameters on fluid-solid interaction. The equivalent stress is utilized for presenting the results which is defined based on von Mises criterion,

$$\sigma_{Eq.} = \sqrt{\frac{1}{2}\left[(\sigma_{11}-\sigma_{22})^2 + (\sigma_{11}-\sigma_{33})^2 + (\sigma_{22}-\sigma_{33})^2 + 6(\sigma_{12}^2+\sigma_{23}^2+\sigma_{13}^2)\right]} \qquad \textbf{Eq. 3-1}$$

Where σ_{ij} is the component of the stress tensor defined in equation 3-7. For convenience the equivalent stress will be presented simply by σ in the figures. It should be mentioned that the magnitude of the von Mises should be lower than the yield strength of the material for engineering applications. Finally, the results for all the cases are presented and discussed in details.

3.1 Material properties

The fluid domain is occupied with air and water droplet. The properties of air and water at ambient temperature are summarized in Table 3-1. For the solid substrate two materials with different elasticity are chosen, namely, martensitic stainless steel and Ti-6Al-4V. Table 3-2 summarizes the properties for materials.

Fluid properties	Air	Water
Density (kg/m^3)	1	1000
Kinematic viscosity (m^2/s)	1.48e-05	1e-06
Surface tension (N/m)	-	0.07

Table 3-1: Fluid properties.

Solid properties	Stainless Steel	Ti-6Al-4V
Density (kg/m^3)	7850	4430
Poisson ratio	0.3	0.342
Young's modulus (GPa)	200	113

Table 3-2: Solid properties.

3.2 Test cases

Several cases were chosen to address the influence of various parameters on drop-substrate interaction. The impact velocity varies between 10-40 m/s and the droplet sizes of 0.5 and 1 mm are selected to investigate any dependence on the drop size. The thicknesses of the solid substrate are 2.5, 5.0 and 10.0 mm. The solid materials are martensitic stainless steel and Ti-6Al-4V, herein referred to as SS and Ti, respectively. Hence, various test cases are created by combination of the abovementioned variables and summarized in Table 3-3.

Solid material	Impact velocity, V (m/s)	Drop size, D (mm)	Thickness th, (mm)
SS	10	0.5	2.5
Ti	20	1.0	5.0
	40		10.0

Table 3-3: Test cases.

3.3 Results

Figure 3-1 illustrates the profile of the liquid droplet as it impacts the solid substrate. The substrate material is stainless steel, impact velocity is 10 m/s, droplet diameter is 0.5 mm and the substrate thickness is 10 mm. the x and y denote axis of symmetry and the interface, respectively. The droplet has a spherical shape right after impact. At early stage of the impact, the droplet deformation occurs fast and after that it gradually spreads over the surface. The spreading continues until the drop forms a thin sheet and completely wets the surface.

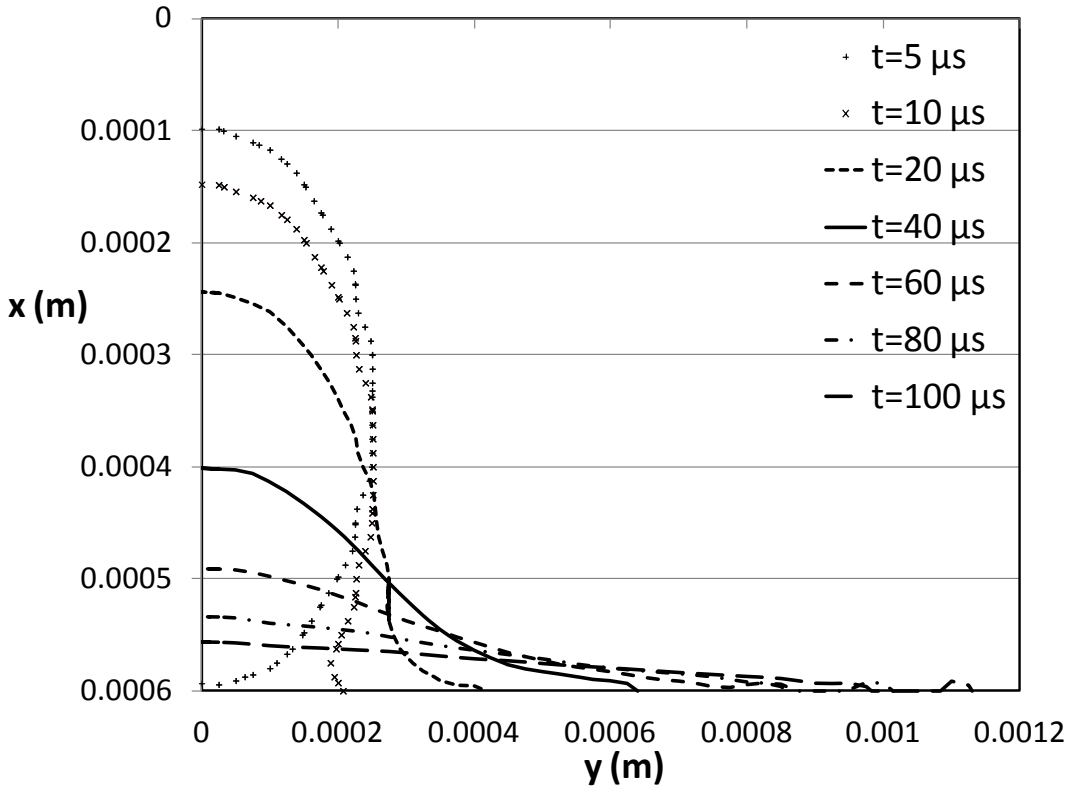

Figure 3-1: Droplet profile evolution upon impact (SS, V=10m/s, D=0.5 mm, th=10 mm).

The radial variation of the fluid pressure and the solid stress on the interface are illustrated in Figure 3-2 and Figure 3-3, respectively. The pressure pulse generated in the liquid 5 µs after impact has a Gaussian distribution and becomes flattened at later times as the droplet spreads over the interface. At 10 and 20 µs the maximum pressure occurs at the droplet edge rather than the center. After 40 µs the pressure again shows a bell-shaped distribution and its magnitude decreases until it becomes almost zero after 100 µs. It should be mentioned that the influence radius of the pressure increases over time with a maximum of 0.5 mm for this case which is the same as the initial drop diameter. The solid stress, on the other hand, shows a completely different behavior compared to the pressure distribution. At early stage of the impact, the stress magnitude is lower than the pressure magnitude and is concentrated around the center axis. As the droplet spreads over the surface, the stress oscillations grow in magnitude and reach up to 0.46 Mpa after 40 µs. The peak transient stress is shifted radially outward and zone of influence on the interface is constantly expanding over time. The stress waves propagate early after impact beneath the interface in the solid and travel radially outward. The stress magnitude is low in the beginning, however, it becomes significant after 40 µs and again it becomes very small after 100 µs.

The maximum values of equivalent stress in the solid and the maximum pressure in the fluid are plotted over time along the solid-fluid interface and center axis in Figure 3-4 and Figure 3-5, respectively. The pressure acting on the interface builds up a few micro-seconds after the impact and reaches its peak value, 0.2 Mpa, after 6 µs. The pressure degrades gradually after this time and approaches zero as the droplet spreads over the surface. The solid response follows the pressure pattern at early stage of impact although with lower values. However, the solid stress increases again and large oscillations are observed which grow in amplitude and reach a

maximum of 0.9 Mpa at 104 µs. the stress amplitude diminishes after this time. The pressure waves generated by the pressure pulse on the interface provoke stress waves in the solid disk. These stress waves travel at both radial and axial directions with the sound speed of the solid. The interaction of the solid waves at certain points leads to appearance of high stresses in solid. The magnitude of the peak transient stress is of importance as it may reach the critical stress of the material and cause severe damage in the solid. The pressure at the center axis of the droplet has similar pattern to the pressure distribution along the interface, i.e., reaching the peak value of 0.2 Mpa and then diminish gradually. The stress behavior on the other hand, is completely different. The solid stress reaches its maximum at 11 µs which is 5 µs after the pressure peak. The stress magnitude in the center axis of solid reaches up to 71.6 Mpa which is much higher than the peak transient stress below the interface which is 0.9 Mpa. After this peak, the transient stress decreases gradually and approaches a steady state value of 0.1 Mpa. This amplitude difference which is about three orders in magnitude indicates the importance of capturing the peak transient stress rather than its steady state value.

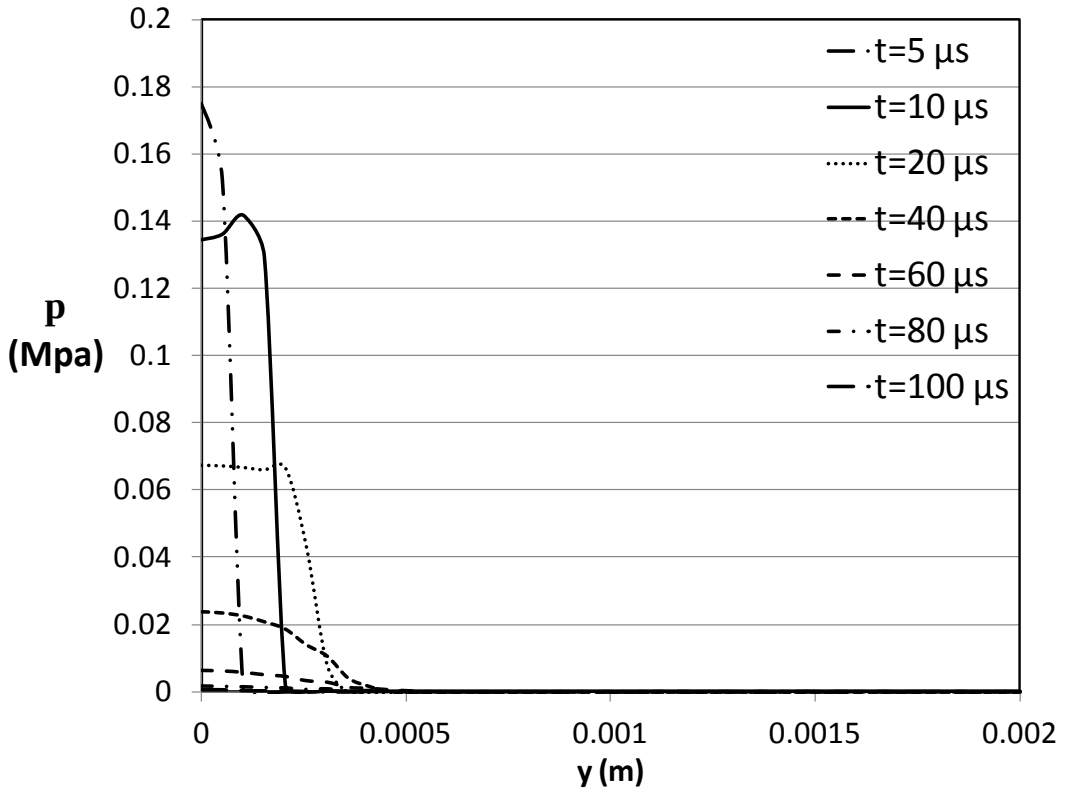

Figure 3-2: Pressure distribution in the liquid along the interface (SS, V=10m/s, D=0.5 mm, th=10 mm).

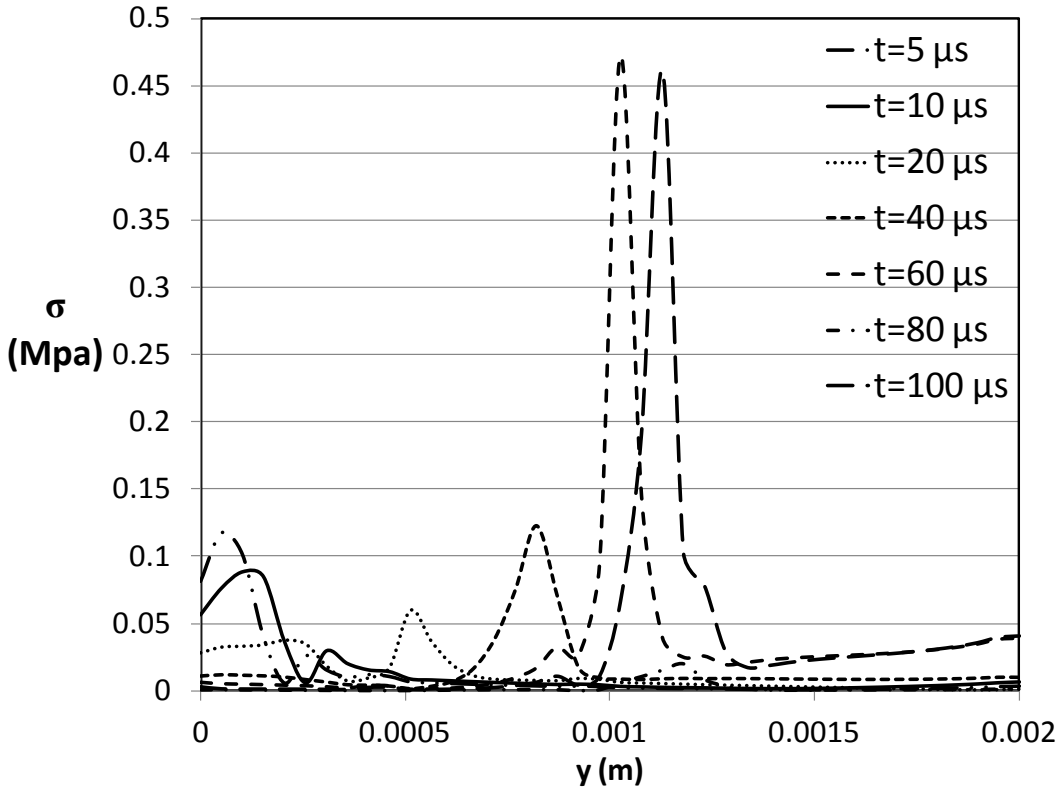

Figure 3-3: Stress in the solid along the interface (SS, V=10m/s, D=0.5 mm, th=10 mm).

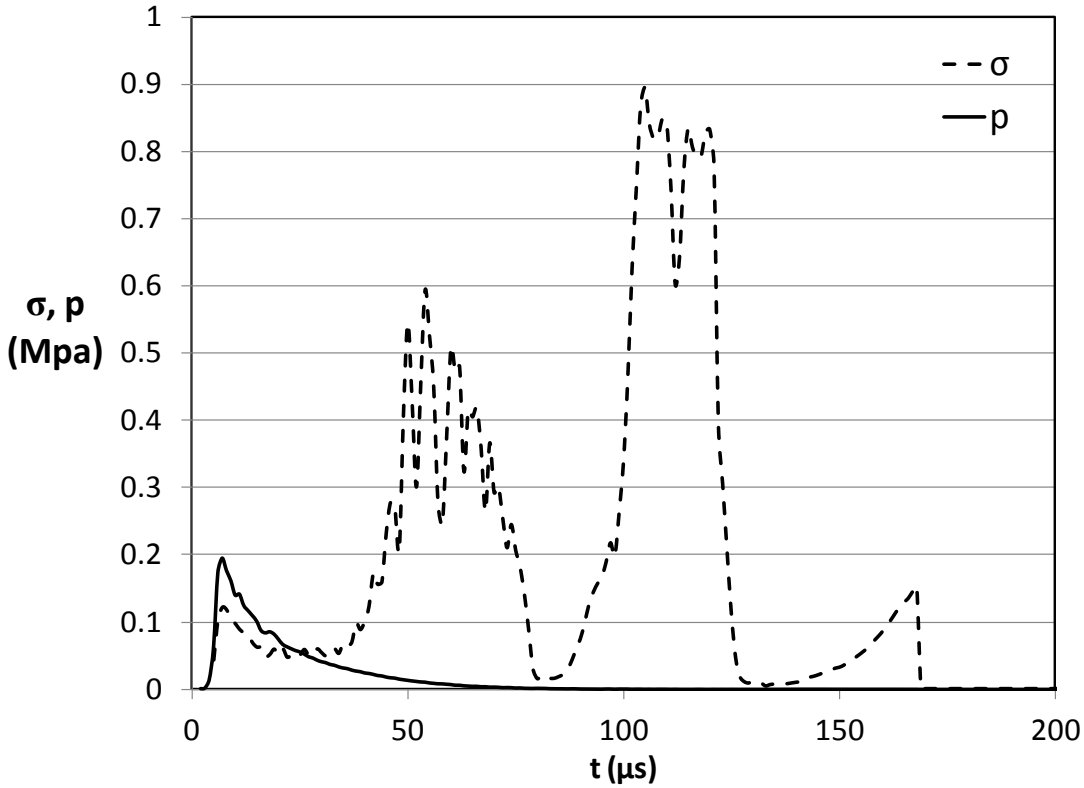

Figure 3-4: Peak transient stress in the solid and maximum pressure in the liquid along the interface (SS, V=10m/s, D=0.5 mm, th=10 mm).

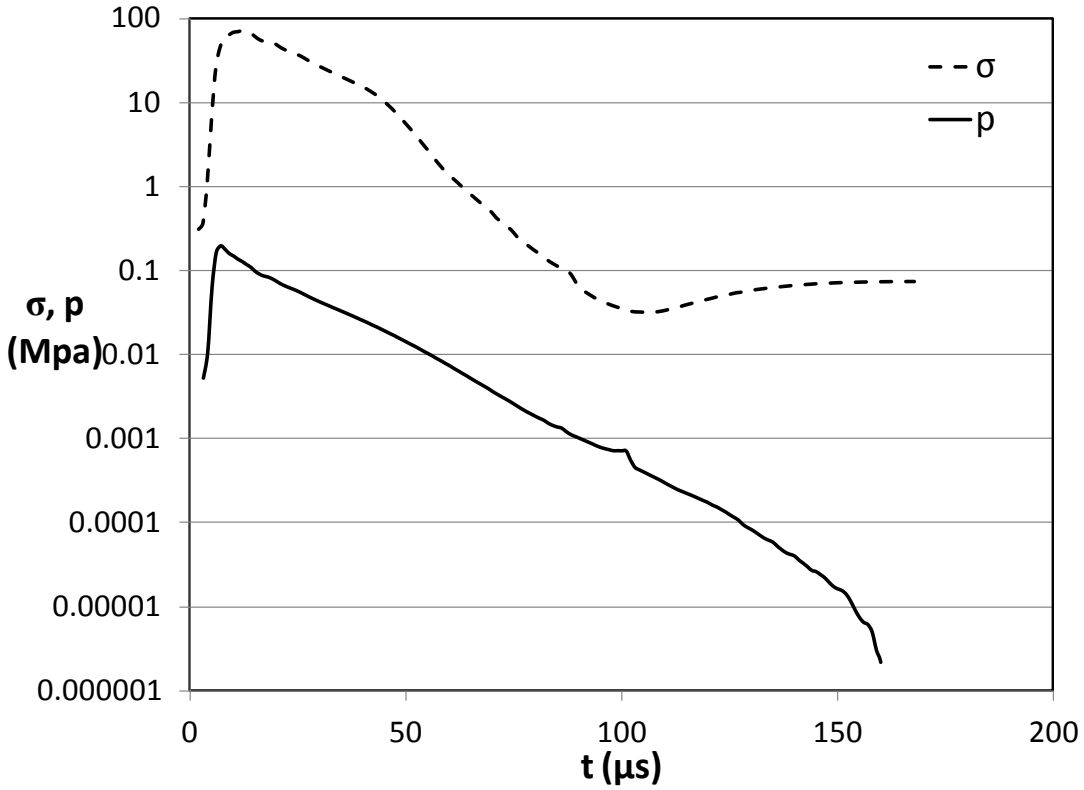

Figure 3-5: Peak transient stress in the solid and maximum pressure in the liquid along the axis (SS, V=10m/s, D=0.5 mm, th=10 mm). Note: vertical axis is shown in logarithmic view.

So far different aspects of the drop impact phenomenon were described for the same case. In the following parts each variable is tackled independently and the rest of the variables are kept constant. The results are divided into sub-sections to address each parameter separately.

3.3.1 Effect of impact velocity

The impact of a 0.5-mm drop is modeled for velocities of 10, 20 and 40 m/s. The thickness of the substrate is 10 mm. The maximum pressure in the liquid region along the solid-fluid interface, Γ_0, is plotted in Figure 3-6. The behavior of the pressure distribution for these three impact velocities is similar, however, with minor differences. The peak pressure appears sooner as the impact velocity is increased, this time is 3 and 2 μs for impact velocities of 20 and 40 m/s, respectively. The value of the peak transient stress is increased to 0.8 and 2.4 for impact velocities of 20 and 40 m/s, respectively. The pressure for the highest impact velocity, i.e. 40 m/s, does not show a gradual decrease and rather oscillates a few times before approaching zero, although the amplitudes are much smaller than the maximum value (is it due to the solid response?). The solid response to the excitations exerted by the pressure force on the solid-fluid interface is illustrated in Figure 3-7. It can be seen that the peak transient stress is oscillatory for all the cases. The maximum amplitude of the oscillations first increases and then diminishes after certain time. The maximum stress has higher magnitude for higher impact velocity; however, there is no consistent pattern in the fluctuations. Figure 3-8 illustrates the maximum pressure in the liquid region along the center axis. The peak pressure along the axis increases significantly from 0.2 MPa for impact velocity of 10 m/s to 0.8 and 2.7 MPa for impact velocities of 20 and

40 m/s, respectively. The time when peak transient pressure appears decreases as the impact velocity is increased. Moreover, the influence time is shorter for higher impact velocities, i.e., the pressure becomes zero faster as the impact velocity increases. The behavior of the peak transient stress along the center axis is shown in Figure 3-9 which is very similar to the maximum pressure. However, the stress magnitude is much higher than the pressure. The peak stress reaches a maximum of 71, 276 and 1320 MPa for impact velocities of 10, 20 and 40 m/s, respectively. The yield strength of martensitic stainless steel is around 1400 Mpa, hence, the impact velocity of 40 m/s is very close to the critical impact velocity. The high compressive stress magnitude can deform the substrate since the solid disk is fixed at its edge. The displacement of the solid disk at its center axis is obtained and used to monitor the substrate deformation. The maximum deformation of the substrate at its center, δ, is plotted over time for the three velocities illustrated in Figure 3-10. It can be seen that the deflection is very small for impact velocity of 10 m/s and increases enormously as the impact velocity increases. The frequency of the oscillations is low and the amplitude diminishes over time. For the highest impact velocity, i.e. 40 m/s, the maximum deflection reaches up to 30 nm which is still considered small. It would be interesting to express the deformation in terms of strain and add strain rates as well.

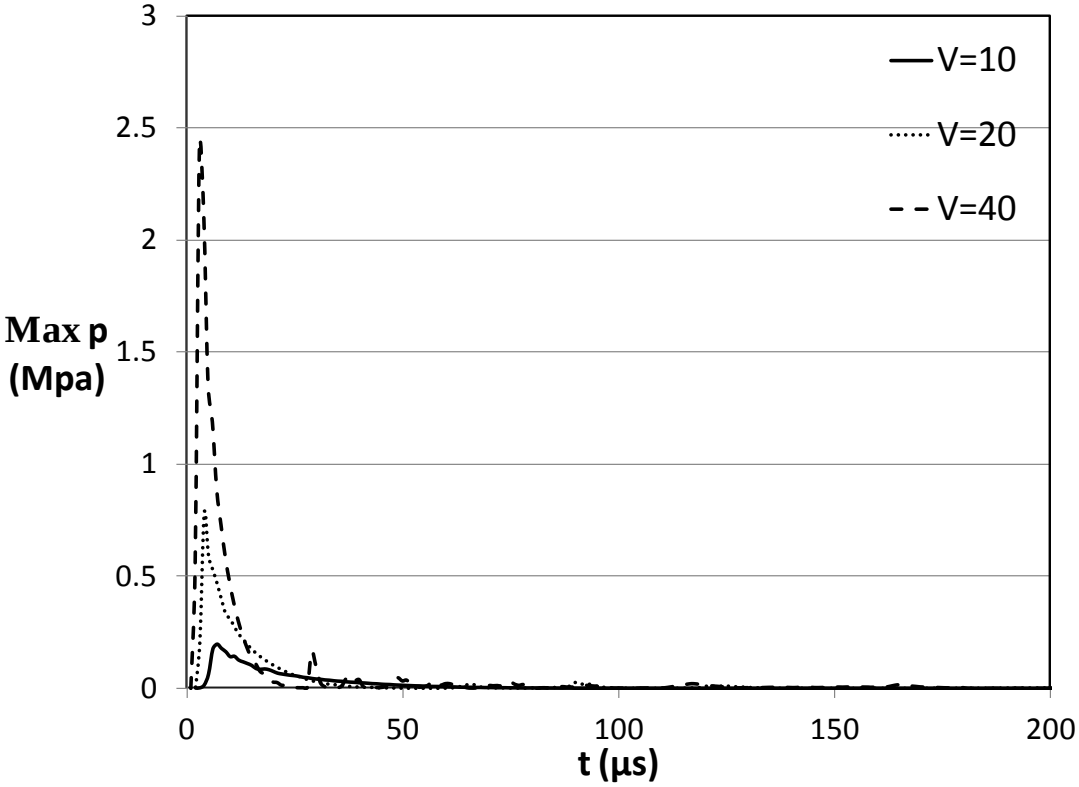

Figure 3-6: Maximum pressure in the liquid along the interface (SS, D=0.5 mm, th=10 mm).

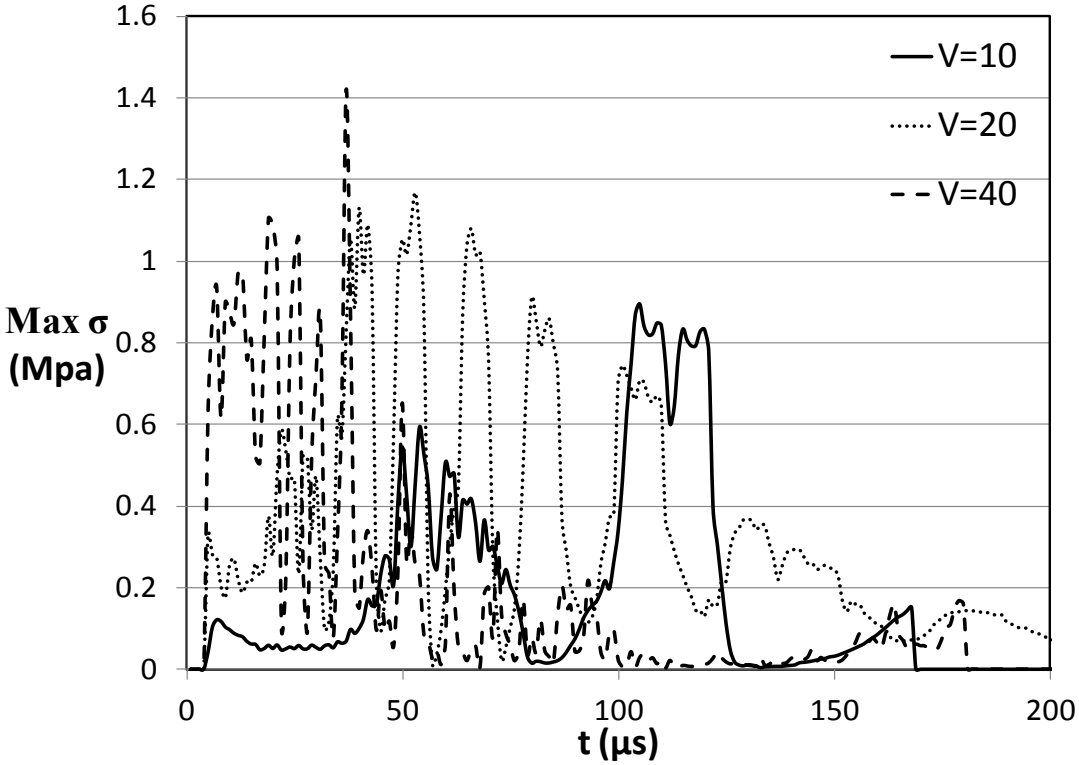

Figure 3-7: Peak transient stress in the solid along the interface (SS, D=0.5 mm, th=10 mm).

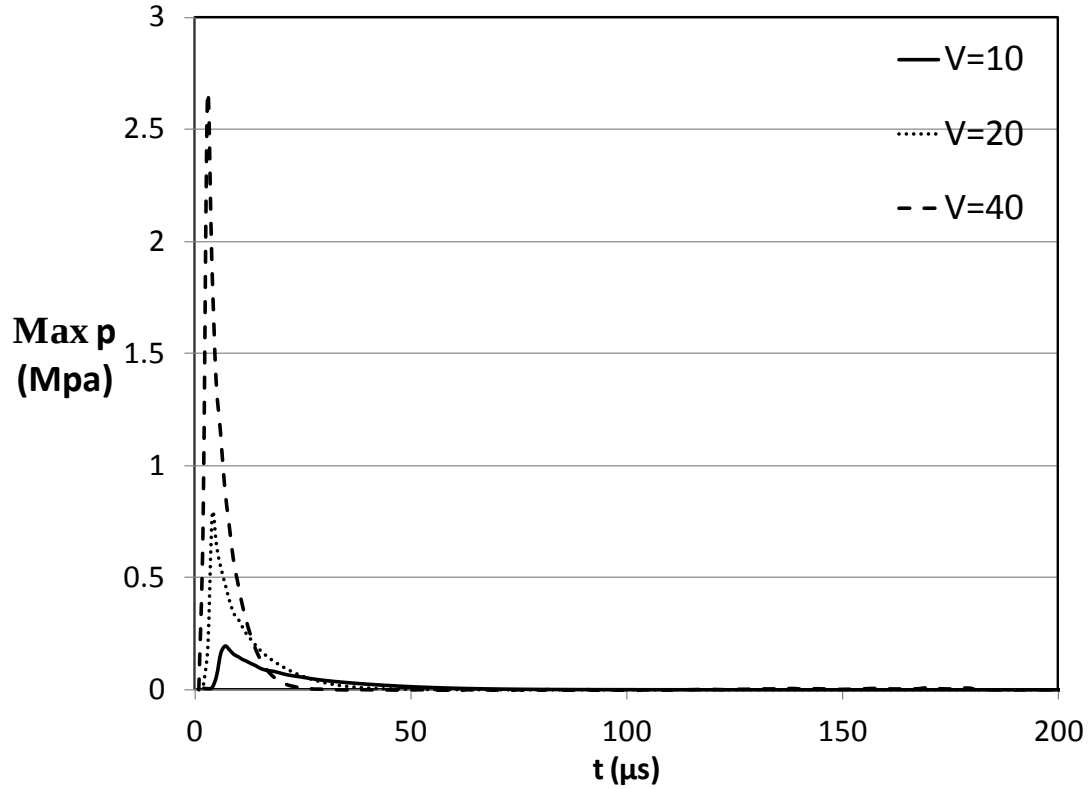

Figure 3-8: Maximum pressure in the liquid along the axis (SS, D=0.5 mm, th=10 mm).

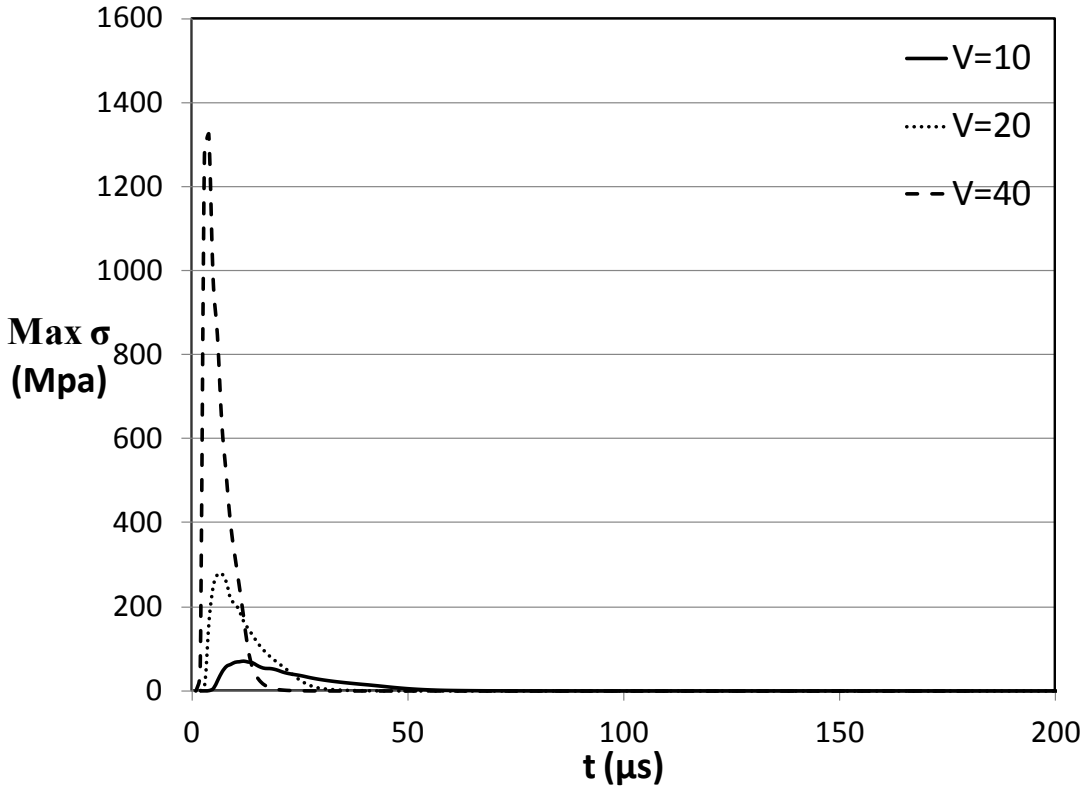

Figure 3-9: Peak transient stress in the solid along the axis (SS, D=0.5 mm, th=10 mm).

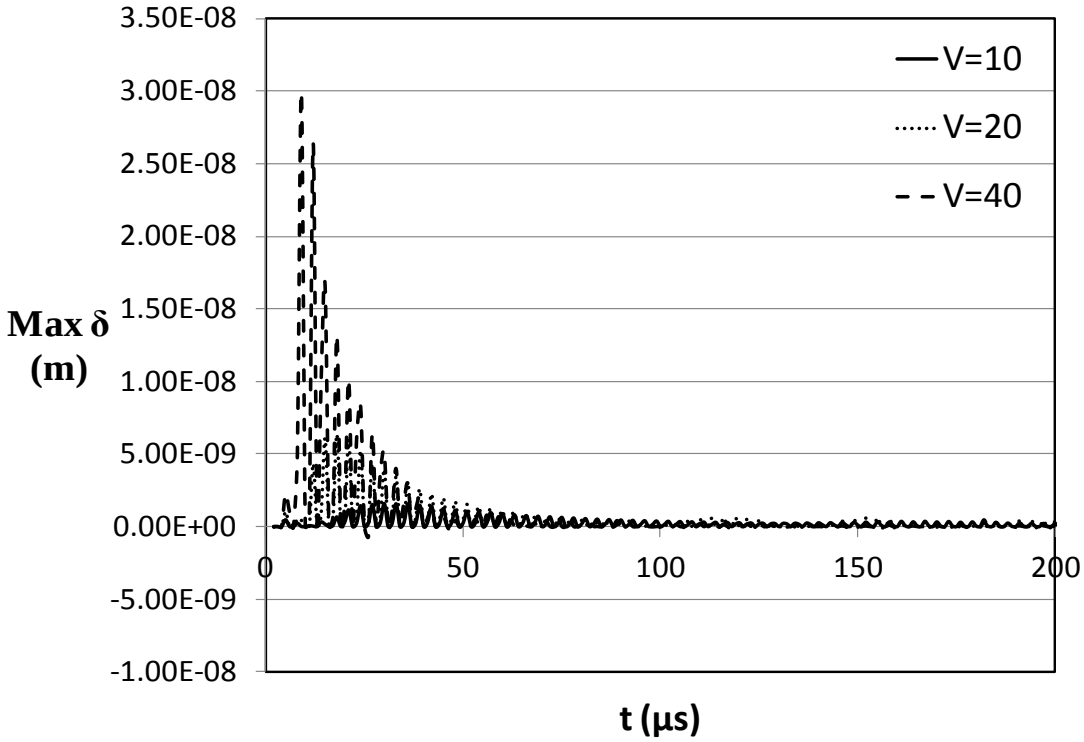

Figure 3-10: Maximum deflection of the solid disk at the center axis over time (SS, D=0.5 mm, th=10 mm).

3.3.2 Effect of substrate thickness

The thicknesses of 2.5, 5.0 and 10.0 mm are selected to study the dependence of the stress distribution on the disk thickness. The impact velocity for all three cases is 10 m/s, the drop diameter is 0.5 mm and the solid material is stainless steel. The maximum pressure along the interface is very similar for the three substrates in magnitude up to about 30 μs. The pressure gradually approaches zero after this time for the 10-mm and 5-mm substrates. On the other hand, the pressure starts to fluctuate on the 2.5-mm substrate and again shoots up. The fluctuations continue until about 70 μs and diminish after that. The stress magnitude along the interface is higher for the thinner substrate early after impact although the pressure values are very similar. This indicates that the stress level is increased when the substrate thickness is lower. However, this difference is only observed until 50 and 70 μs for the 10-mm and 5-mm substrates and after these times the stress magnitudes are approximately the same. The peak stress magnitude for 10-mm and 5-mm substrates reaches its maximum value, i.e. 71 and 117 Mpa respectively, and drops quickly. For the 2.5-mm substrate the maximum stress is 149 Mpa and fluctuates for a period of time before convergence to zero. The oscillations of the disk center are small until 100 μs and grow in amplitude after this time up to 0.37 microns. The maximum deflection is considerably higher for the 2.5-mm substrate compared to two other substrates.

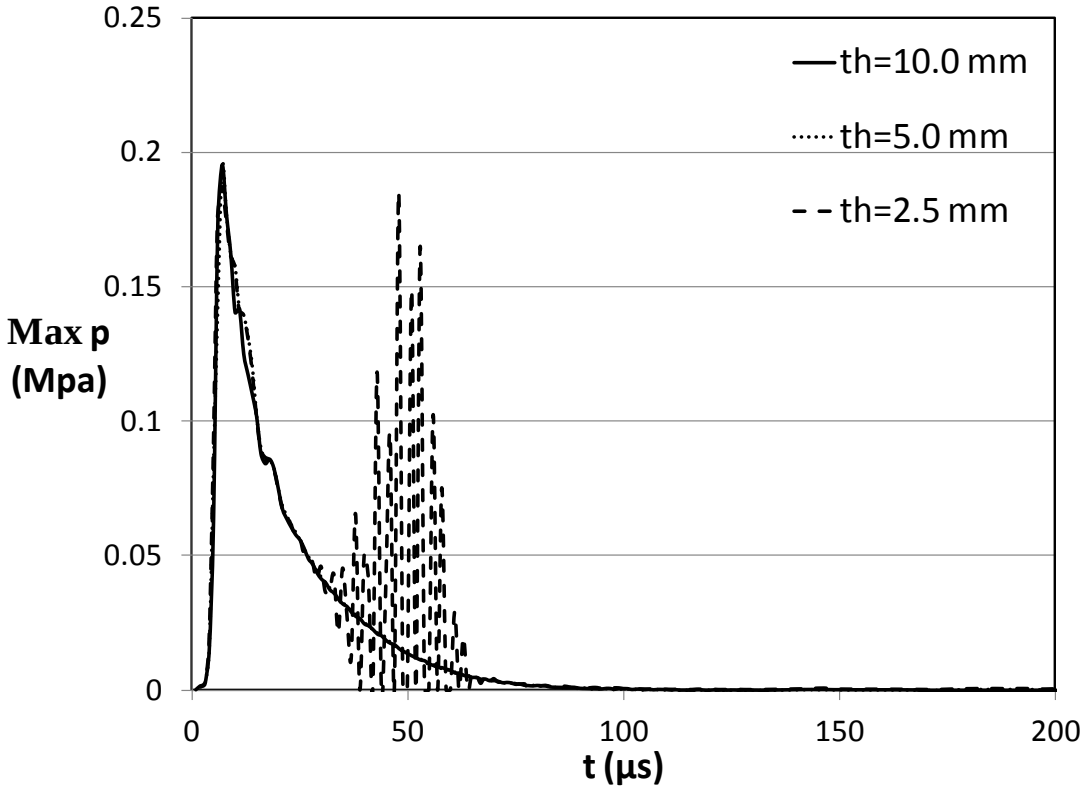

Figure 3-11: Maximum pressure in the liquid along the interface (SS, V=10m/s, D=0.5 mm).

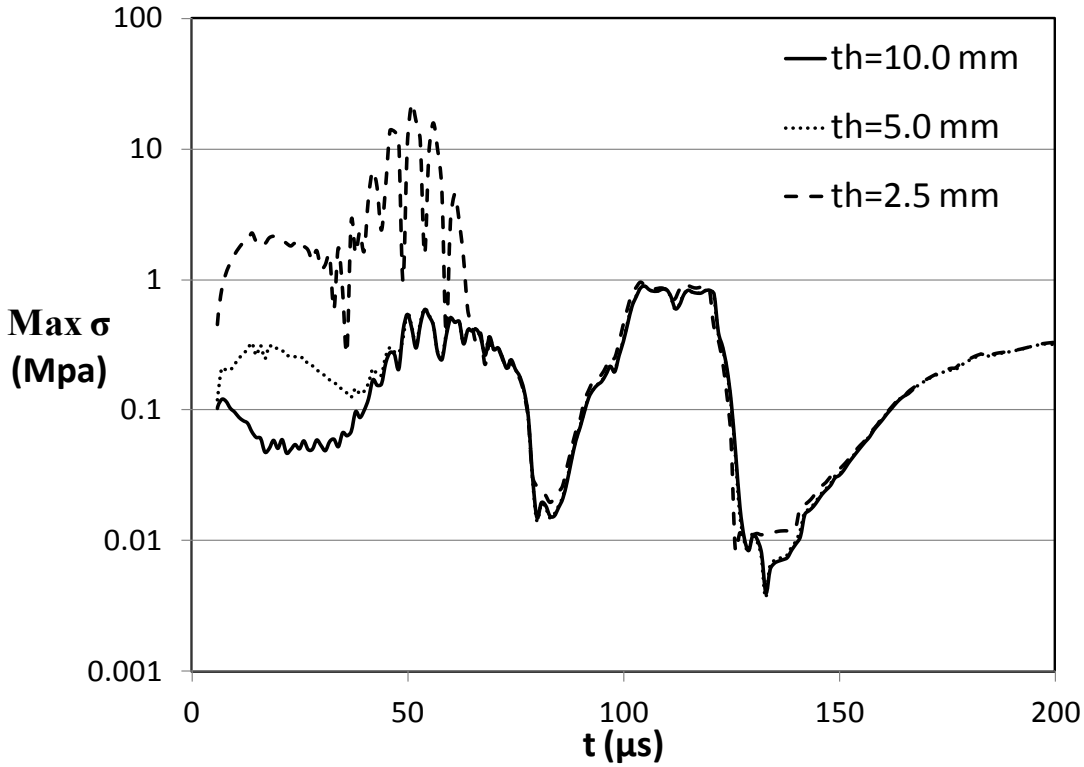

Figure 3-12: Peak transient stress in the solid along the interface (SS, V=10m/s, D=0.5 mm). Note: vertical axis is shown in logarithmic view.

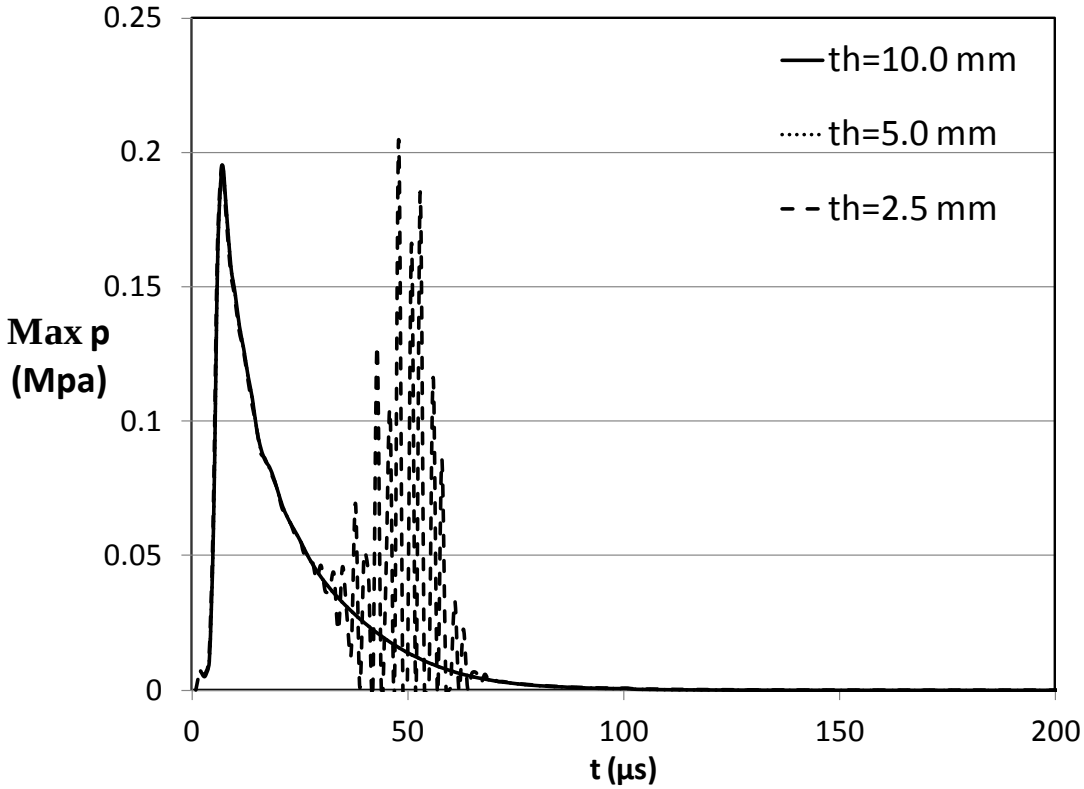

Figure 3-13: Maximum pressure in the liquid along the axis (SS, V=10m/s, D=0.5 mm).

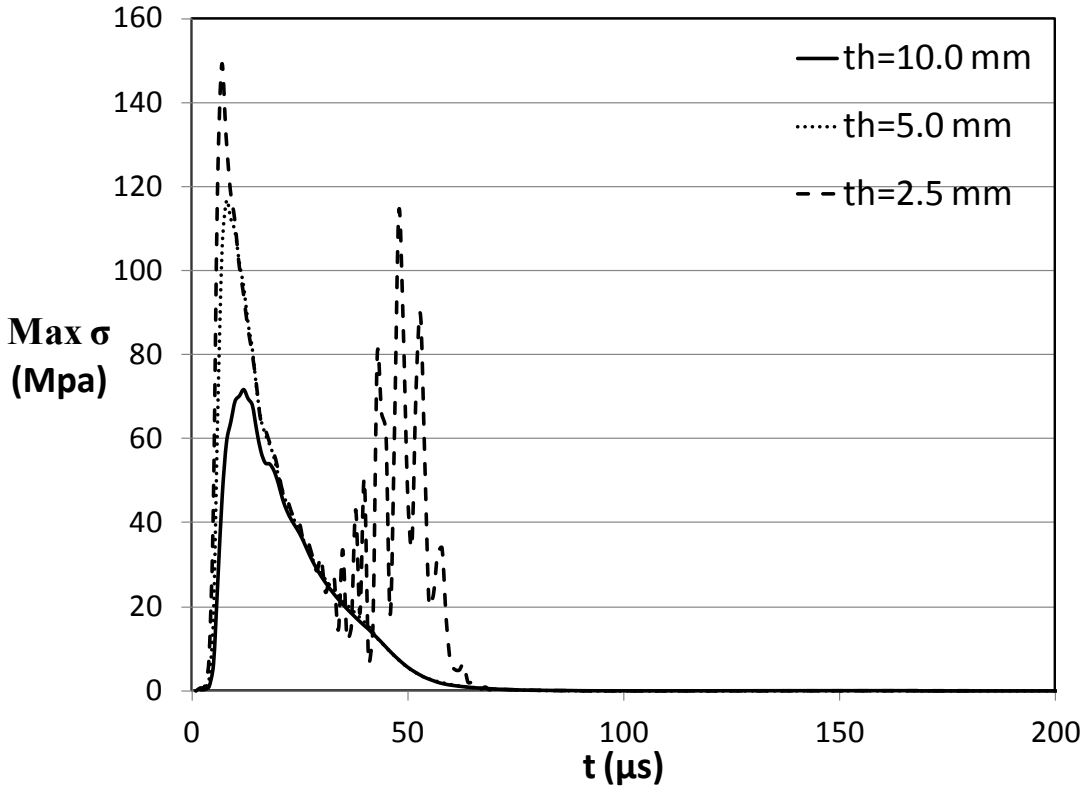

Figure 3-14: Peak transient stress in the solid along the axis (SS, V=10m/s, D=0.5 mm).

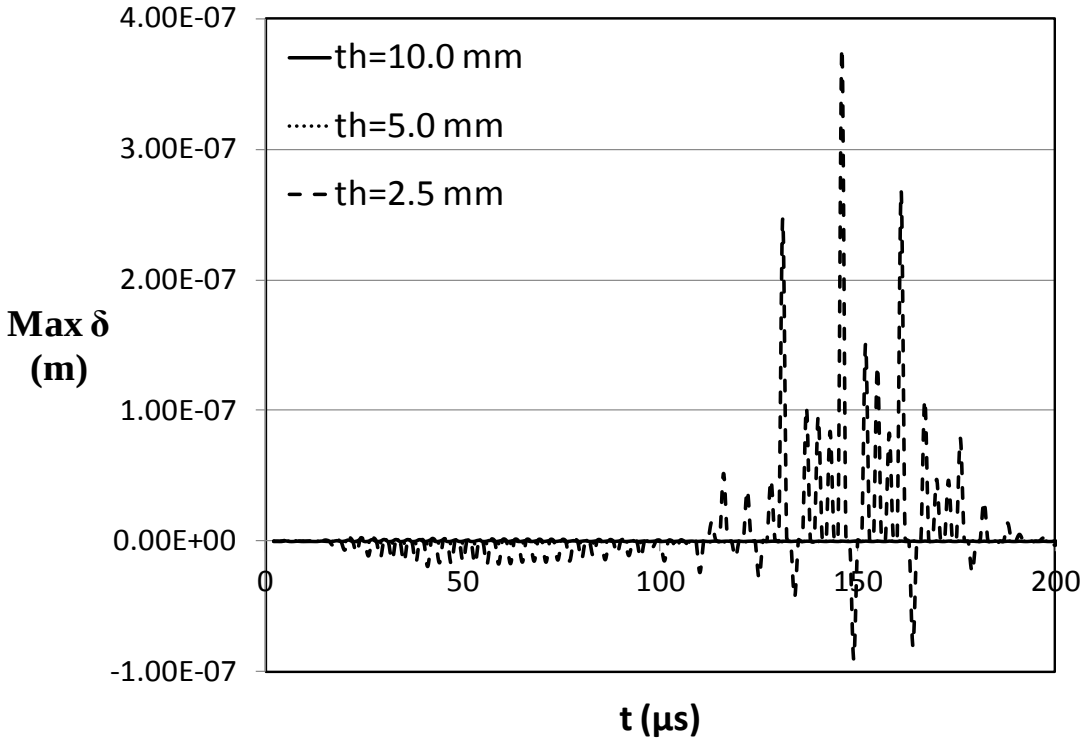

Figure 3-15: Maximum deflection of the solid disk at the center axis over time (SS, V=10m/s, D=0.5 mm).

3.3.3 Effect of droplet size

To investigate the effect of droplet diameter on the stress and pressure levels, two drop sizes of 0.5 and 1 mm are compared against each other. The substrate thickness is 10 mm and the impact velocity is 10 m/s. The pressure for both diameters has the same magnitude with a time lag for 1-mm droplet. The transient stress below the interface behaves differently although the pressure magnitude was almost equal for two drop diameters. The peak stress generated by the impact of 1-mm droplet has higher values compared to 0.5-mm drop until about 50 µs. After this time, the stress fluctuations for the case of 0.5-mm droplet grow in amplitude and shoot up to 0.9 Mpa. On the other hand, the pressure shows similar behaviors along the axis for both cases and the time lag is still visible. The maximum pressure along the axis is increased from 0.19 to 0.22 Mpa for larger droplet and the maximum stress is increased from 71 to 135 Mpa. The deflection caused by 0.5-mm droplet diminishes faster than 1-mm drop. In general, the amplitude of oscillations is larger for 1-mm droplet compared to 0.5-mm drop.

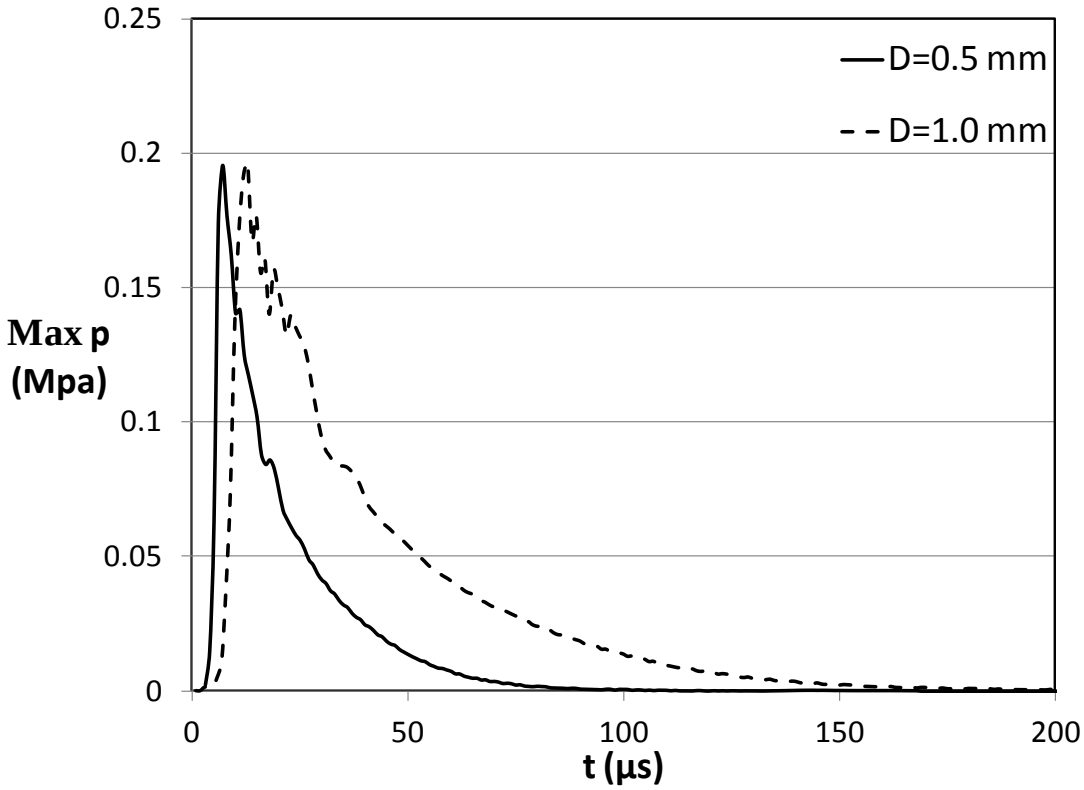

Figure 3-16: Maximum pressure in the liquid along the interface (SS, V=10m/s, th=10 mm).

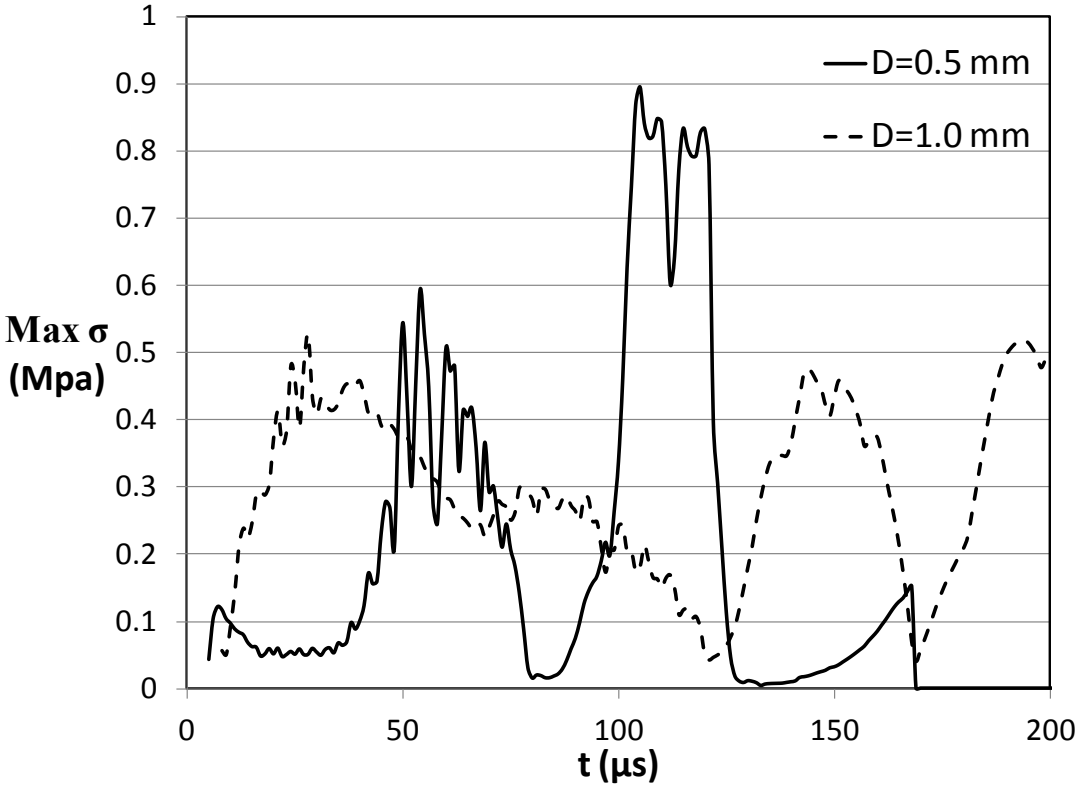

Figure 3-17: Peak transient stress in the solid along the interface (SS, V=10 m/s, th=10 mm).

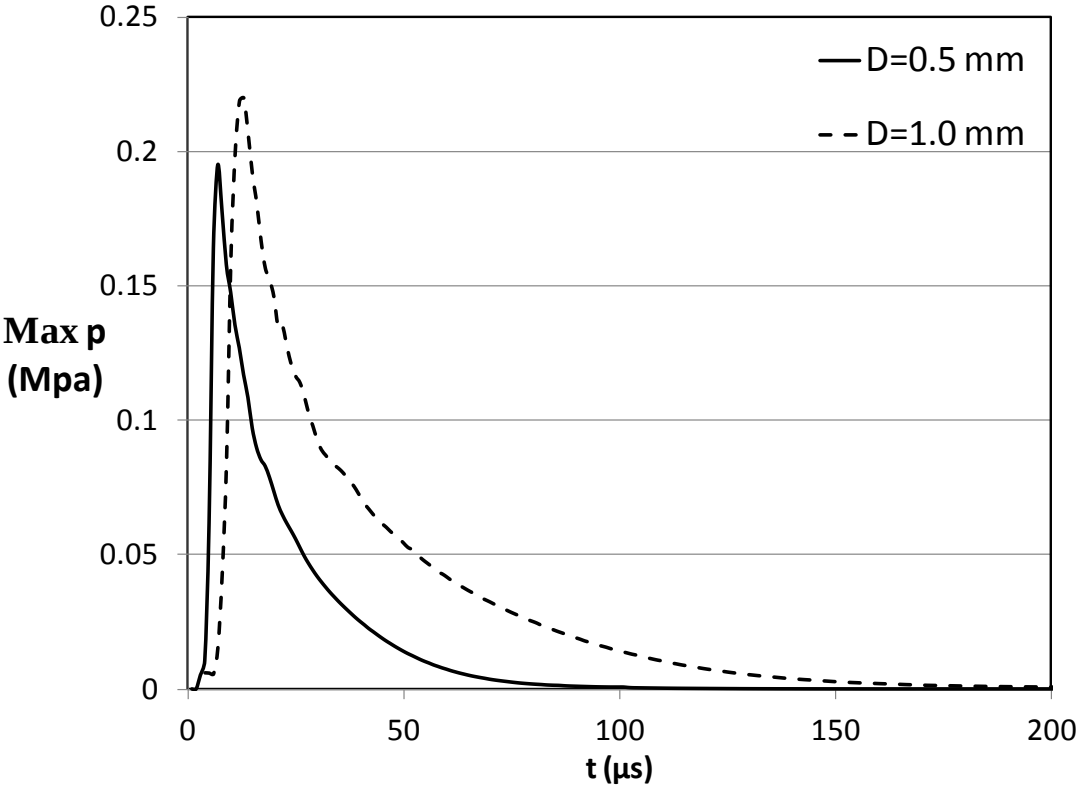

Figure 3-18: Maximum pressure in the liquid along the axis (SS, V=10m/s, th=10 mm).

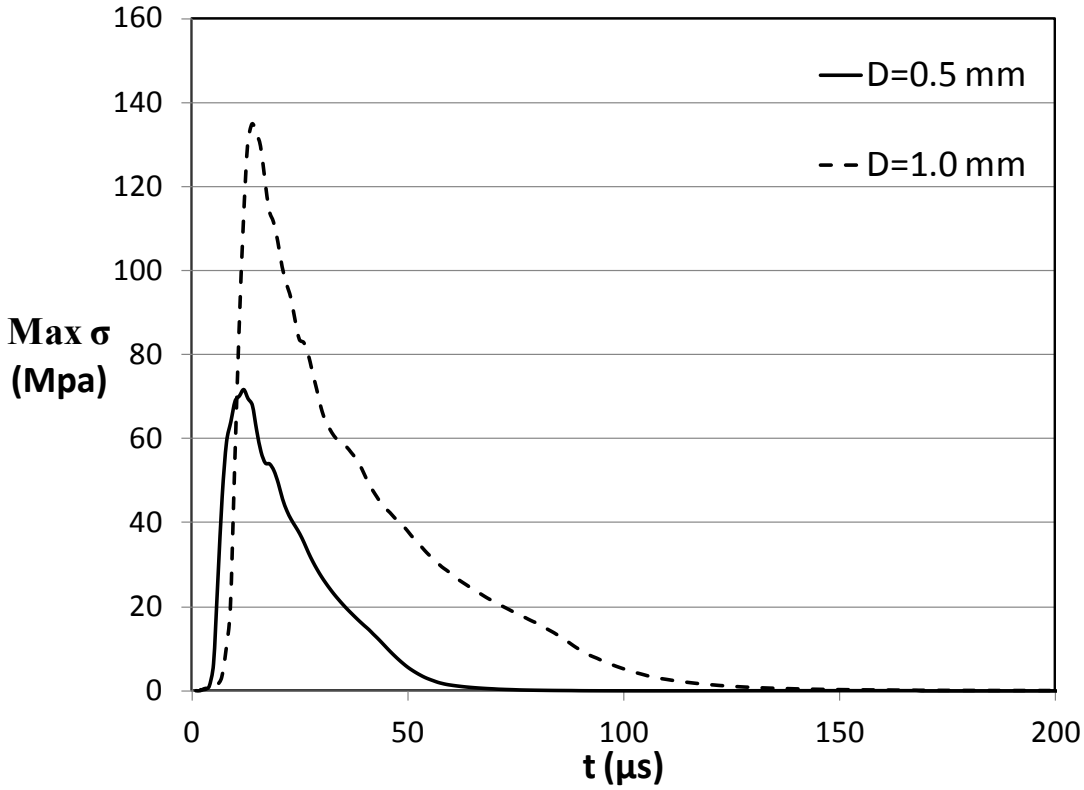

Figure 3-19: Peak transient stress in the solid along the axis (SS, V=10m/s, th=10 mm).

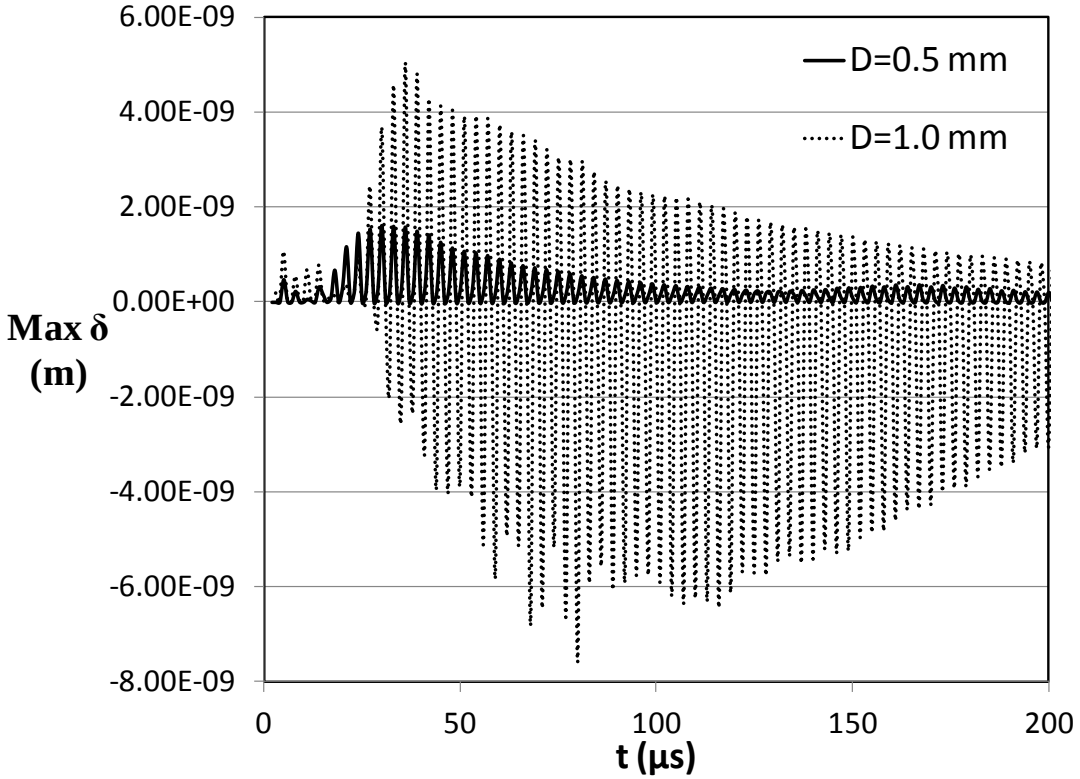

Figure 3-20: Maximum deflection of the solid disk at the center axis over time (SS, V=10m/s, th=10 mm).

3.3.4 Effect of solid elasticity

Two materials are chosen for the simulations; martensitic stainless steel and Ti-6Al-4V. Ti-6Al-4V has similar Poisson ratio compared to stainless steel, however, its Young's modulus is about half of that for stainless steel. Substrate thickness of 10 mm and impact velocities of 10 and 20 m/s are used for both cases. The results reveal that the pressure distribution along the interface is almost the same and very similar along the axis except for Ti is slightly higher. The stress magnitude has approximately the same value both on the interface and axis with a time delay for Ti. The maximum deflection shoots up early after impact for Ti plate and becomes small. The oscillations for the second time grow in amplitude and gradually degrade over time. the fluctuations become large again after 150 μs. The frequency of oscillations is very similar for both materials; however, the amplitudes of fluctuations for Ti are higher than that of SS.

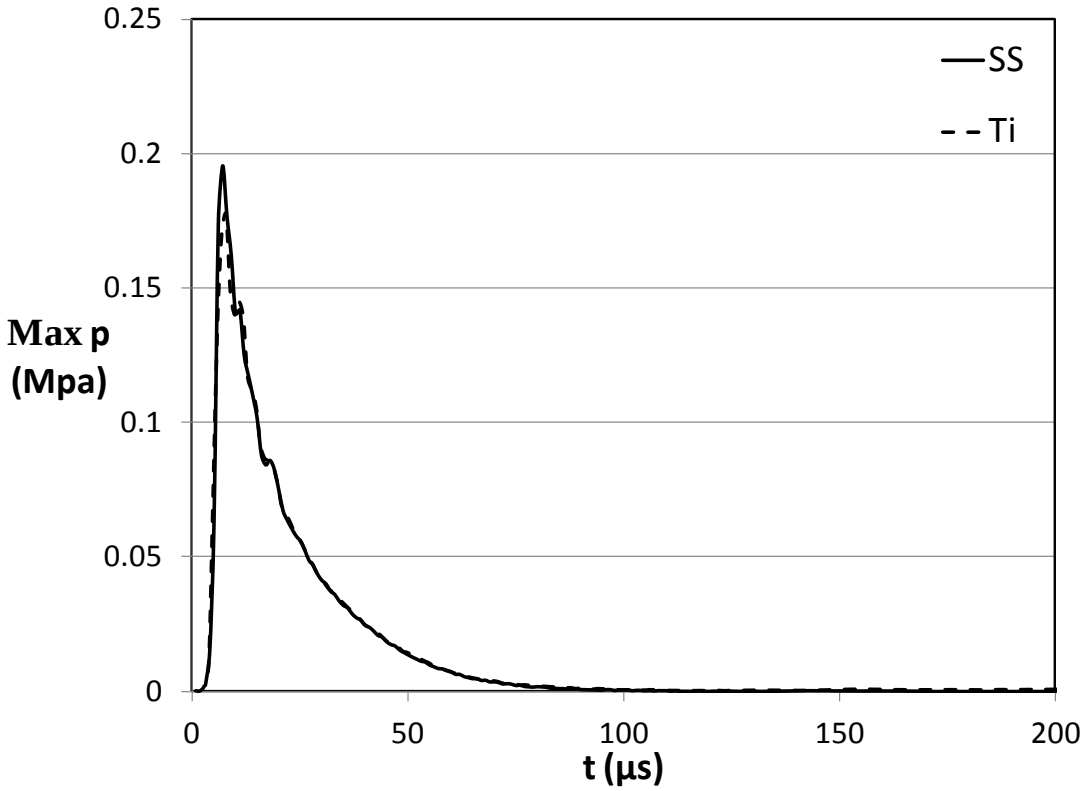

Figure 3-21: Maximum pressure in the liquid along the interface (V=10m/s, D=0.5 mm, th=10 mm).

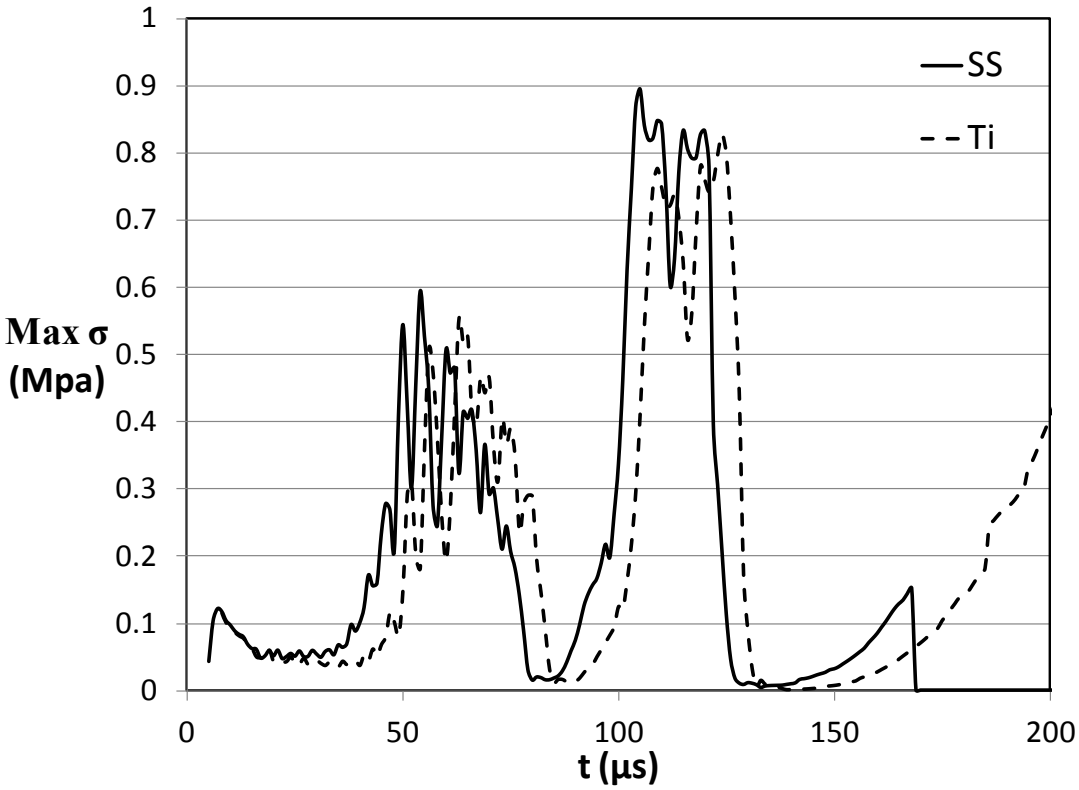

Figure 3-22: Peak transient stress in the solid along the interface (V=10m/s, D=0.5 mm, th=10 mm).

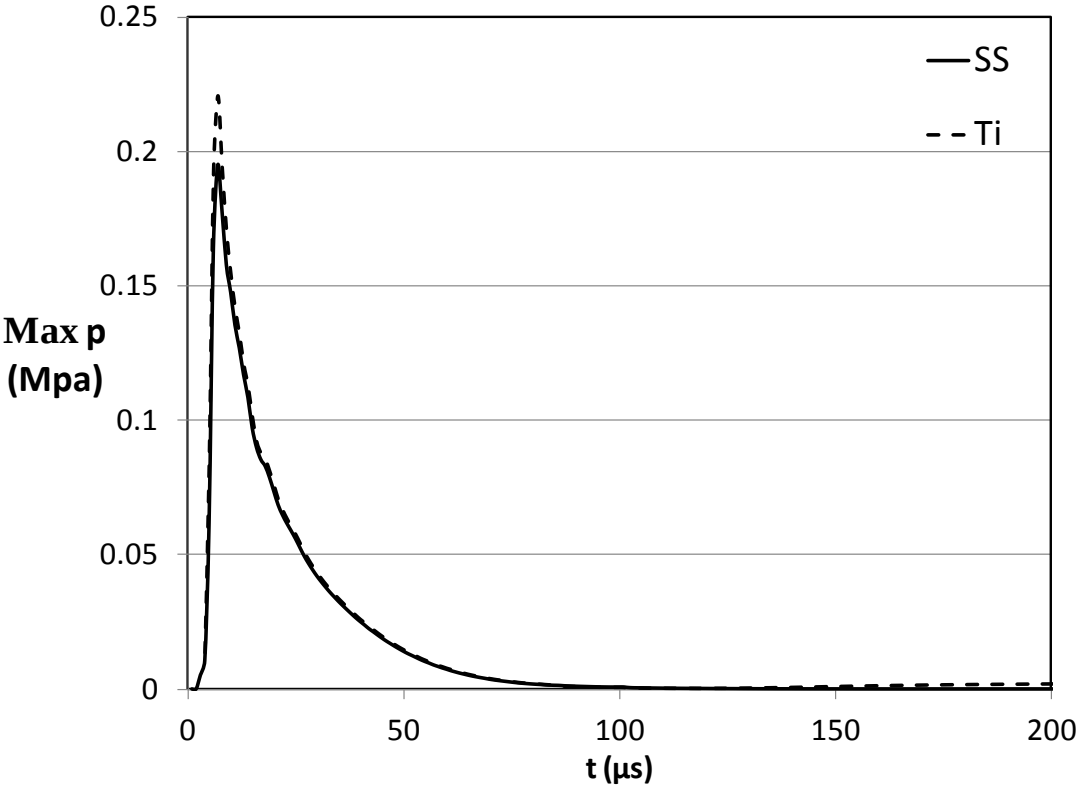

Figure 3-23: Maximum pressure in the liquid along the axis (V=10m/s, D=0.5 mm, th=10 mm).

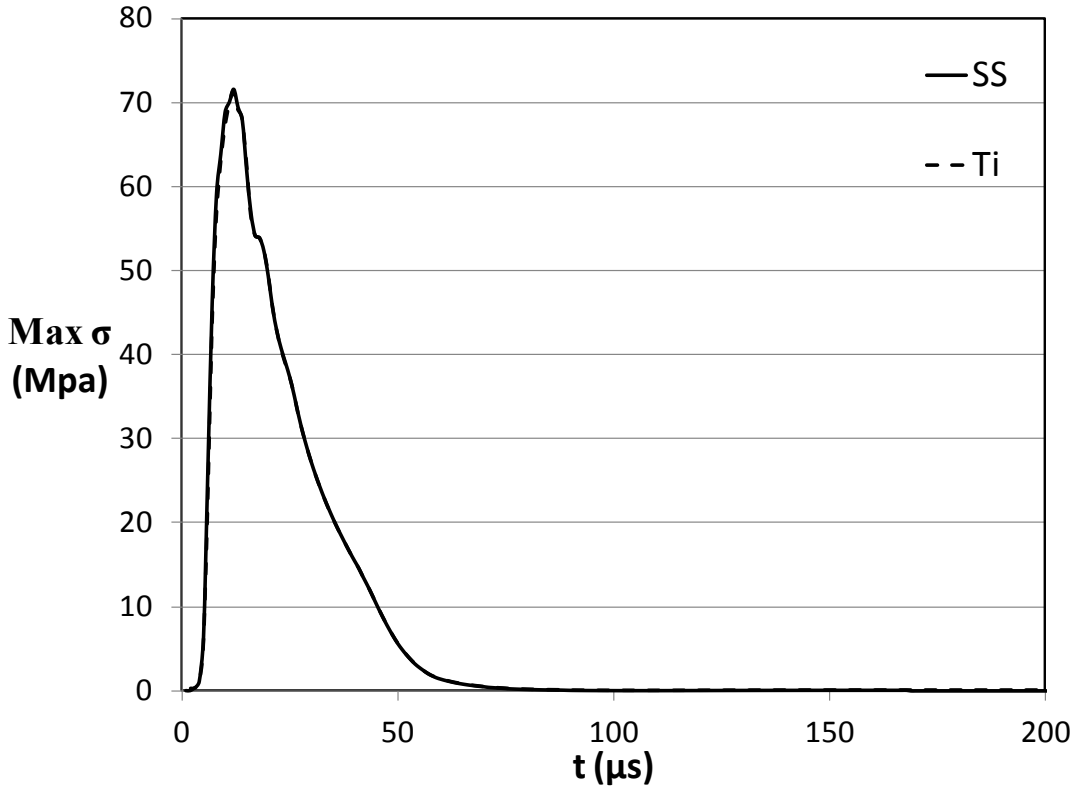

Figure 3-24: Peak transient stress in the solid along the axis (V=10m/s, D=0.5 mm, th=10 mm).

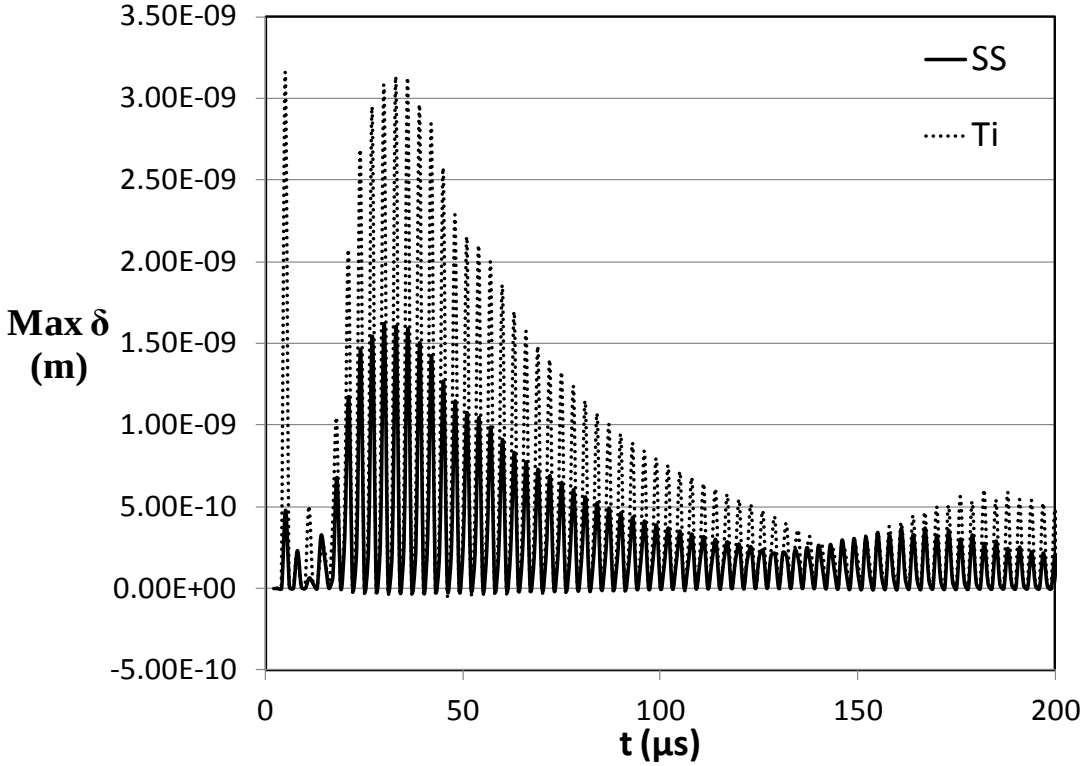

Figure 3-25: Maximum deflection of the solid disk at the center axis over time (V=10m/s, D=0.5 mm, th=10 mm).

3.3.5 Tensile stress

In order to illustrate the appearance of tensile stress in the solid, the impact velocity of 40 m/s, stainless steel substrate with the thickness of 2.5 mm and droplet diameter of 0.5 mm are selected. The negative values for xx-stress component (σ_{11}) correspond to the compressive stresses in the solid. The compressive stress is highest below the solid surface (x=0.0006 m) and sharply reduces to zero along the axis. The magnitude of the compressive stress diminishes rapidly after 10 µs and becomes almost zero at 60 µs. This time designates the end of loading stage for the impact and after this time tensile stress appears in the solid. The positive values of σ_{11} confirm the appearance of tensile stress in the solid as earlier reported by Zhang *et al* [16]. The maximum magnitude of the tensile stress in this case is 0.13 Mpa (is it the same stress distribution in all directions?) which is very small compared to the magnitude of compressive stress with a maximum of 1220 Mpa at 5 µs. Although small in magnitude, the tensile stress can become of importance if the impacts are repetitive and fatigue type of failure is expected.

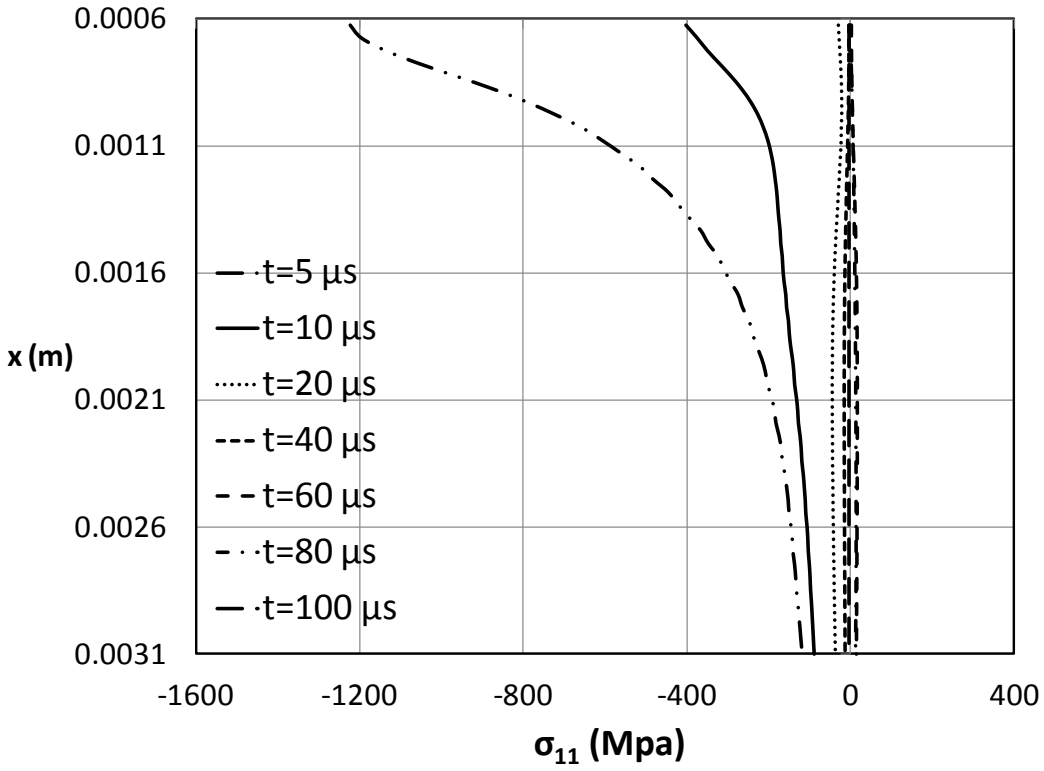

Figure 3-26: xx-stress component in the solid along the axis (SS, V=40m/s, D=0.5 mm, th=2.5 mm).

4 Concluding remarks

4.1 Conclusions

The impact of a liquid droplet onto an elastic solid disk was studied in this work. The important parameters affecting fluid-solid interaction were identified and tackled separately. The droplet curvature and deformation was captured by VOF method at each time step. The coupled fluid

and solid equations were solved together in order to obtain the liquid pressure and solid stress simultaneously. The results revealed that the pressure force acting on the interface has a Gaussian shape early after impact and flattens over time. This change in pressure is concurrent with the droplet deformation and spreading over the surface. The solid response to the pressure history is consistent to the pressure distribution at early stage of impact. However, at later times, large oscillations are observed in the stress magnitude. There was no particular pattern seen in the frequency of oscillations and the amplitude of fluctuations varied over time. The solid stress showed wave-like behavior which propagated upon droplet impact and transmitted along the interface. The stress magnitude captured on the interface was much lower than transient stress along the center axis. The highest stress magnitude was observed right below the interface in the solid and the disk bottom experienced the lowest stress. The peak transient stress appeared shortly after impact and diminished less than 100 μs depending on the impact conditions. This so-called loading stage during which the stress is compressive was then followed by an unloading stage when tensile stresses were observed in the solid. The magnitude of the tensile stress was very low compared to the compressive stress. The excitation force deflected the substrate and this deflection was calculated as a function of time. It can be concluded that the peak transient stress and substrate deflection increase by increasing the impact velocity or initial droplet diameter. On the other hand, increasing the disk thickness results in the reduction of the maximum stress magnitude and deflection. From stress point of view, both SS and Ti disks behave similarly; however, the deflections are larger for Ti substrate.

4.2 Comparison with previous works

The peak transient stresses obtained from the simulations are compared to the previous results in the literature shown in Figure 4-1. In both studies the substrate material is martensitic stainless steel and three impact velocities are selected for comparison. The work of Li *et al.* [15] was based on a 2-D axisymmetric model focusing on acoustic stage of impact, normally less than 100 ns. They reported that the peak stress magnitude is independent of the droplet diameter. The substrate thickness effect was not discussed in their study. The droplet size for these simulations is 0.5 mm and the substrate thickness is 10 mm. In general the peak transient stresses predicted by present work are much higher than that of Li *et al*. [15]. The essential difference between two works lays on the fluid governing equation. Li *et al*. [15] solved the wave equation for incompressible and compressible liquid and assumed the drop deformation is negligible. On the other hand, full Navier-Stokes equations are solved for incompressible fluid in the present work. To the best of author's knowledge, no experimental results were reported on this issue and analytical solutions are limited to generalized cases of liquid column impact. Hence, the validation of any numerical study on this subject is not achievable to date.

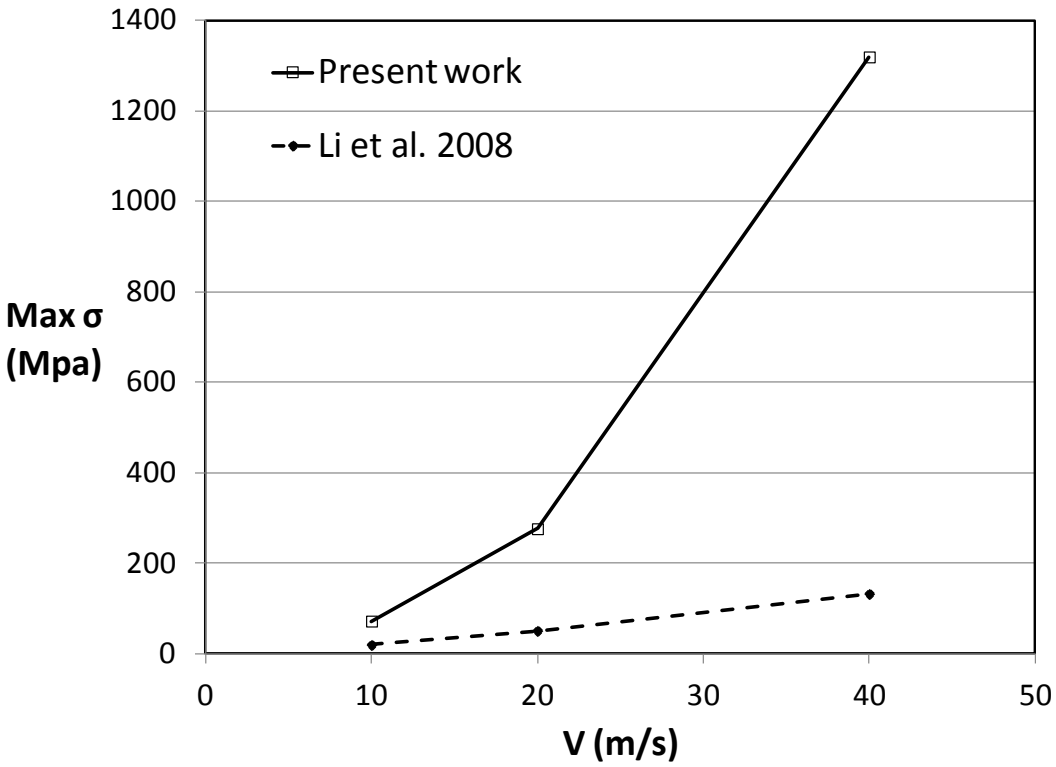

Figure 4-1: Comparison between the results of present work and literature.

5 References

1. *Essais d'érosion des ailettes de turbines à vapeur.* **Honegger, E.** Baden : Revue BBC, 1927, Vol. 14, pp. 95-104.

2. *The Mechanics of Erosion by Liquid and Solid Impact.* **Bargmann, Heinz W.** 1415, s.l. : International Journal of Solid Structure, 1992, Vol. 29, pp. 1685-1698.

3. *Erosion by liquid impact.* **Springer, G. S.** Washington DC : Scripta Publishing Company,Wiley, 1976.

4. *Test on Erosion caused by Jets.* **Honegger, E.** s.l. : Brown Boveri Review, 1927, Vol. 14, pp. 95-104.

5. *Erosion by Water Hammer.* **Cook, S. S.** s.l. : Proceeding of the Royal Society, 1928, Vol. 119, pp. 481-8.

6. *Waterdrop Collisions with Solid Surface.* **Engel, O. G.** s.l. : Journal of Research of the National Bureau of Standards, 1955, Vol. 54.

7. *On the Response of an Elastic Solid to Droplet Impact.* **Blowers, R. M.** s.l. : International Journal of the Institute of Mathematics and Its Applications, 1969, Vol. 5, pp. 167-193.

8. *Analysis of Water Drop Impacts on Layered Window Constructions.* **Adler, W. F. and Mihora, D. J.** s.l. : Proceedings of the SPIE 2286, 1994, pp. 264-274.

9. *Computational Study of High-speed Liquid Droplet Impact.* **Haller, K. K., et al.** s.l. : Journal of Applied Physics, 2002, Vol. 92, pp. 2821-8.

10. *Hydrodynamic phenomena during high-speed collision between liquid droplet and rigid plane*. **Huang, Y. C., Hammitt, F. G. and Yang, W. J.** s.l. : Journal of Fluids Engineering, 1973, Vol. 95, pp. 276-294.

11. *The thoeretical investingation and experimental research on the water drop impact destroy of blades in the wet steam turbine stage.* **Shih, H.** s.l. : Ph.D.thesis, Xi'an Jiaotong University, Xi'an, China, 1989.
12. *Mechanisms governing the high temperature erosion of thermal barrier coatings used in gas turbines.* **Chen, X., et al.** s.l. : Wear, 2004, Vol. 256, pp. 735-746.
13. *Stress Wave Propagation in a Coated Elastic half-space due to Water Drop Impact.* **Kim, H. S., et al.** s.l. : Transactions of the ASME, 2001, Journal of Applied Mechanics, Vol. 68, pp. 346-8.
14. *Ananalysis of stress waves in 12Cr steel, Stellite 6B and TiN by liquid impact loading.* **Lee, M. K., et al.** s.l. : Nuclear Engineering and Design, 2002, Vol. 214, pp. 183-193.
15. *Liquid drop impact on solid surface with application to water drop erosion on turbine blades, Part I: Nonlinear wave model and solution of one-dimensional impact.* **Li, Na, et al.** s.l. : International Journal of Mechanical Sciences, 2008, Vol. 50, pp. 1526-1542.
16. *Liquid drop impact on solid surface with application to water drop erosion on turbine blades, Part II: Axisymmetric solution and erosion analysis.* **Zhou, Qulan, et al.** s.l. : International Journal of Mechanical Sciences, 2008, Vol. 50, pp. 1543-1558.
17. **Suresh, S.** *Fatigue of Materials.* New York : Cambridge University Press, 1998.
18. *Time-Dependent Multi-Material Flow with Large Fluid Distortion.* **Youngs, D. L.** [ed.] K. W. Morton and M. J. Baines. s.l. : Academic Press, 1982, Numerical Methods for Fluid Dynamics.
19. **Turek, S. and Hron, J.** Proposal for Numerical Benchmarking of Fluid-Structure Interaction between an Elastic Object and Laminar Incompressible Flow. [book auth.] H-J. Bungartz and M. Schäfer. *Fluid-Structure Interaction.* s.l. : Springer, 2006.
20. *High-speed photography of surface geometry effects in liquid/solid impact.* **Dear, J. P. and Field, J. E.** s.l. : Journal of Applied Physics, 1988, Vol. 63, pp. 1015-21.
21. *High-speed impact between a liquid drop and a solid surface.* **Heymann, F. J.** s.l. : Journal of Applied Physics, 1969, Vol. 40, pp. 5113-22.
22. *The Effects of Target Compliance on Liquid Drop Impact.* **Field, J. E., Dear, J. P. and Ogren, J. E.** s.l. : Journal of Applied Physics, 1989, Vol. 65, pp. 533-40.